UCRL-9990

University of California

Ernest O. Lawrence Radiation Laboratory

Berkeley, California

DISCLAIMER

Paper to be presented by Gerson Goldhaber at
1962 International Conference on High Energy Physics at CERN

UCRL-9990

UNIVERSITY OF CALIFORNIA

Lawrence Radiation Laboratory
Berkeley, California

Contract No. W-7405-eng-48

K^+-p INTERACTION FROM 140 TO 642 MeV/c

Sulamith Goldhaber, William Chinowsky, Gerson Goldhaber,
Wonyong Lee, Thomas O'Halloran, Theodore Stubbs,
G. M. Pjerrou, Donald H. Stork, and Harold K. Ticho

May 29, 1962

K^+-p INTERACTION FROM 140 TO 642 MeV/c*

Sulamith Goldhaber, William Chinowsky, Gerson Goldhaber,
Wonyong Lee, Thomas O'Halloran, Theodore F. Stubbs,

Lawrence Radiation Laboratory
University of California
Berkeley, California

and

G. M. Pjerrou, Donald H. Stork, and Harold K. Ticho

Department of Physics
University of California
Los Angeles, California

May 29, 1962

A detailed investigation of the energy dependence of the K^+-proton scattering cross section at low momenta has been carried out. In the region from 140 to 642 MeV/c, the nuclear cross section varies little with energy. The cross sections are distinctly lower than values quoted earlier.[1] The momentum dependence of the phase shifts below 300 MeV/c can only be interpreted as s-wave scattering and does not admit isotropic p-wave solutions such as were obtained as possible ambiguities at 810 MeV/c.[2] The isotropy in the differential cross sections and the constructive interference with Coulomb scattering at each of the momenta show that the repulsive s-wave character of the K^+-p $T = 1$ state persists throughout this region.

An s-wave effective-range fit to the experimental K^+-p data up to 642 MeV/c gives, for the scattering length, $a = -0.29 \pm 0.015$ fermi and, for the effective range, $r_0 = 0.5 \pm 0.15$ F. It should be noted that for the highest momentum included in the fit, the quantities $|ak|$ and r_0k remain below unity. Alternatively, the data can also be represented by a purely repulsive core of radius $r_c = 0.31 \pm 0.01$ F.

The experimental data for this analysis were obtained from photographs taken with the 15-inch LRL bubble chamber. A mass-separated K^+ beam described earlier[2] was conveyed by a beam transport system at 645 MeV/c. Figure 1 shows the mass resolution curve for this momentum. The background of light particles (pions, muons, and electrons) was approximately 0.5%. The method of analysis of the data at 642 MeV/c is very similar to that described earlier.[2] At this momentum only about 0.5% of the total cross section, or about 0.06±0.03 mb, is due to inelastic pion production.[3]

Four distinct series of pictures taken are described here, the first with the direct K^+ beam giving 642±7 MeV/c in the chamber and three more with various thicknesses of tungsten absorbers placed immediately ahead of the chamber. This gave average momenta of 520±15, 355±25, approximately 220 MeV/c, respectively. At the lowest-momentum series the initial spread of the beam as well as the energy loss in the absorber and in the chamber liquid yields a K-meson path-length distribution over the momentum interval from zero to 300 MeV/c. Since the path length falls off rapidly at the edges of the momentum distribution, we have accepted for the purpose of cross-section determinations a momentum band from 120 to 280 MeV/c, which we divided into five momentum intervals.

In all the momenta bands but the lowest, only tracks satisfying a predetermined angular criterion were accepted. At the lowest momentum we accepted all tracks entering the bubble chamber window, irrespective of angle. To permit the measurements of interaction products with sufficient accuracy, only those interactions occurring in a restricted volume (referred to as fiducial volume FV) were accepted. The acceptance criteria were applied after the measurements were completed.

The momenta of all K-H interactions were determined by kinematical fitting at the interaction point. The path lengths contributing to the various momentum intervals were computed from the number of "tau" decays in flight, their known mean life, and K^+ branching ratio into this decay mode. For this purpose all three-prong "tau-like" decays were measured. From kinematical fitting it was possible (a) to select the true τ-meson mode, and (b) to get an accurate momentum at which the τ decay occurred.[4] At the lowest momentum band (120 to 280 MeV/c), where the path-length distribution was particularly critical, we measured 10% of all tracks and obtained the path-length distribution from the measured momentum distribution and the measured track lengths. This provided an additional method independent of the τ-decay distribution.

The experimental differential cross sections are shown in Fig. 2. We have taken a cutoff at a scattering angle corresponding to $\cos\theta_{cm} = 0.95$, beyond which detection efficiencies decrease rapidly. The repulsive K^+-N potential is evident at all momenta, and, in particular, in the lowest momentum interval, where the constructive interference with Coulomb scattering is most striking.

The isotropic character of the K^+-p differential cross section can be fitted for any single momentum interval by (a) pure s-wave scattering, (b) $p_{1/2}$-wave scattering, and (c) a suitable mixture of $p_{1/2}$- and $p_{3/2}$- wave scattering. These ambiguities were discussed in detail in our earlier work at 810 MeV/c.[2] However, with the series of momenta we have available now, it becomes clear that the p-wave solutions can be ruled out. In particular at momenta below 300 MeV/c the phase-shift behavior disagrees clearly with p waves, i.e., $\tan\delta \propto k^3$. Furthermore, the variation of δ with momentum is smooth up to 810 MeV/c, hence a switchover to one of the p-wave solutions appears extremely unlikely.

The differential cross sections were computed by using pure s-wave and Coulomb scattering amplitudes:

$$\frac{d\sigma}{d\Omega} = \frac{1}{k^2} \left| e^{i\delta_1} \sin\delta_1 - \frac{a}{2\sin^2(\theta_{cm}/2)} \exp\left[-ia\,\ell n \sin^2\left(\frac{\theta_{cm}}{2}\right)\right] \right|^2 , \quad (1)$$

where

$$a = \frac{e^2}{\hbar v_{rel}} ,$$

$\hbar k$ = the center-of-mass momentum, v_{rel} = the relative velocity, and δ_1 = the s-wave phase shift. The continuous curves shown in Fig. 2, a through h, are based on the repulsive s-wave phase shifts.

Table I lists these phase shifts as well as the experimental data from which they were computed. Column 2 gives the total cross section[5] up to $\cos\theta_{cm} = 0.85$. The phase shifts, Column 4, were computed by equating the experimental cross sections with the corresponding integral over Eq. (1). The total nuclear cross sections given in Column 3 have been computed from $\sigma = 4\pi \sin^2 \delta_1/k^2$. The above procedure actually yields two s-wave phase shifts, an attractive and a rupulsive one. For illustration the dashed curve in Fig. 2a shows the differential cross section for the attractive solution $\delta_1 = +10.5°$ fitted up to $\cos\theta_{cm} = 0.6$. It is clear by comparison with the experimental differential cross sections that the attractive solutions can be eliminated. Figure 3 illustrates the behavior of the experimental total cross sections, the total nuclear cross sections, and the repulsive s-wave phase shifts as a function of the momentum in the laboratory system.

We have further shown that the data up to 642 MeV/c can be well represented with a two-parameter effective-range approximation. A least-square fit to the integrated cross sections[6] up to 355 MeV/c with the constraint of $k\cot\delta = \frac{1}{a} + \frac{1}{2} r_0 k^2$ allows the determination of the scattering length to

within less than 10% ($a = -0.29 \pm 0.02$ F), but leaves large uncertainties in the effective range[7] ($r_0 = 0.6 \pm 0.06$ F). In this momentum interval the quantities $|ak|$ and $r_0 k$, which test the validity of the effective-range expansion, remain well below unity. It is remarkable, however, that the values of the parameters hardly change when we include data up to 642 MeV/c in the least-square fit. The values for the scattering length and effective range now become $a = -0.29 \pm 0.015$ F and $r_0 = 0.5 \pm 0.15$ F, respectively,[8] with a goodness of fit (χ^2) corresponding to an 85% probability. It should be noted here that upon inclusion of the higher momenta the uncertainty in r_0 has been decreased appreciably.

Finally we have also attempted to fit the experimental data directly to a phenomenological potential. The potential considered was a repulsive hard core of radius r_c followed by an attractive well of range r_a and depth V.

This gives

$$k \cot(\delta + kr_a) = k' \cot k'(r_a - r_c), \tag{2}$$

where

$$k' = \sqrt{k^2 + 2\mu V}.$$

A least-square fit to the integrated cross sections up to 642 MeV/c with the constraint of Eq. (2) was attempted. We find that the experimental data lack the statistical accuracy needed to determine the three parameters. It should be noted, however, that a one-parameter fit, setting $V = r_a = 0$ and thus reducing Eq. (2) to $\delta_1 = -r_c k$, fits the data up to 642 MeV/c with a 40% probability, giving a hard-core radius $r_c = 0.31 \pm 0.01$ F. These results, as well as the consequences from insisting on a zero-range approximation, are given in Table II.

REFERENCES

* Work done under the auspices of the U. S. Atomic Energy Commission.

1. T. F. Kycia, L. T. Kerth, and R. G. Baender, Phys. Rev. 118, 553(1960).
2. T. F. Stubbs, H. Bradner, W. Chinowsky, G. Goldhaber, S. Goldhaber, W. Slater, D. H. Stork, and H. K. Ticho, Phys. Rev. Letters 7, 188(1961).
3. G. Fisk, D. H. Stork, H. K. Ticho, W. Chinowsky, G. Goldhaber, S. Goldhaber, and T. F. Stubbs (following communication).
4. We were able to utilize this method down to the lowest momentum considered here. Even at $P_K \approx 120$ MeV/c, the separation between a τ decay "at rest" and "in flight" was quite definite.
5. This smaller angle was chosen so as to avoid regions of poorer scanning efficiency. Corrections have been made to the data for scanning bias in the distribution of the azimuthal angle ϕ. The corrections become very small if we stay away from the angles for which $\cos\theta_{cm} > 0.85$.
6. We have shown that the least-square fits are not sensitive to the cutoff angle by varying the latter as well as dividing the data into two angular intervals in the fitting procedure.
7. Here it should be remarked that the two parameters are actually strongly correlated and the errors quoted are the diagonal elements of the error matrix only. The error matrix is $\begin{pmatrix} .00042 & .011 \\ .011 & .344 \end{pmatrix}$.
8. The error matrix is now $\begin{pmatrix} .00014 & .0012 \\ .0012 & .015 \end{pmatrix}$.
9. V. Cook, D. Keefe, L. T. Kerth, P. G. Murphy, W. A. Wenzel, and T. F. Zipf, Phys. Rev. Letters 7, 182 (1961).

Table I. K^+-p cross sections and phase shifts from 140 to 642 MeV/c.

The experimental cross sections are quoted up to a cutoff angle corresponding to $\cos\theta_{cm} = 0.85$. The nuclear cross sections are computed up to $\cos\theta_{cm} = 1$, for pure repulsive s-wave scattering. The last column gives the corresponding phase shifts.

	Experimental	T = 1 S-wave fit	
P_K(MeV/c)	σ nuclear + Coulomb for $\cos\theta_{cm} \leq 0.85$ (mb)	σ Nuclear (mb)	δ_1 (deg)
140 ± 20	14.9 ± 2.5	9.2 ± 2.1	-7.2 ± 0.8
175 ± 15	16.0 ± 2.4	12.5 ± 2.2	-10.4 ± 0.9
205 ± 15	13.7 ± 1.8	11.5 ± 1.7	-11.7 ± 0.9
235 ± 15	12.7 ± 1.6	11.2 ± 1.6	-13.2 ± 0.9
265 ± 15	11.0 ± 1.6	10.0 ± 1.6	-14.0 ± 1.1
355 ± 25	11.9 ± 1.2	11.7 ± 1.2	-20.0 ± 1.1
520 ± 15	11.9 ± 1.2	12.2 ± 1.3	-29.4 ± 1.7
642 ± 7	11.9 ± 0.8	12.4 ± 0.9	-36.2 ± 1.4

Table II. Summary of the effective-range approximation and potential fit to the experimental K^+-p scattering cross section.

Effective range, approximation

Momentum interval (MeV/c)	a (10^{-13} cm)	r_0 (10^{-13} cm)	Probability from a χ^2 Fit
140-355	-0.29±0.02	0.6±0.6	75%
140-642	-0.29±0.015	0.5±0.15	85%

Zero-Range approximation

	a (10^{-13} cm)	r_0 (10^{-13} cm)	
140-355	-0.3±0.01	0	65%
140-642	-.33±0.01	0	1%

Hard Core

	r_c (10^{-13} cm)	
140-642	0.31 ± 0.01	40%

FIGURE CAPTIONS

Fig. 1. Mass analysis of particles emerging from the first slit. This curve was obtained by varying the magnetic field in the second spectrometer. The ordinate gives the current through the spectrometer coils (measured in millivolts across a shunt).

Fig. 2. The differential K^+-p cross section at the various momenta. The solid curves correspond to the differential cross sections computed for repulsive s-wave scattering. The corresponding phase shifts are given in Table I. The dashed curve in Fig. 2a illustrates the effect of an attractive s-wave phase shift fitted up to $\cos\theta_{cm} = 0.6$.

Fig. 3. Variation of the measured cross section with laboratory momentum up to a cutoff angle taken at $\cos\theta_{cm} = 0.85$. Corresponding total nucleon cross sections, computed with a repulsive phase shift. Also given for comparison are the data of Kycia et al. (Ref. 1) and Cook et al. (Ref. 9), as well as our own data at 810 MeV/c (Ref. 2). Repulsive s-wave phase shifts. It should be noted that at 810 MeV/c about 1 mb of inelastic scattering is included (Ref. 2). The solid curves correspond to the effective range fit up to 642 MeV/c, the dashed curves to the fit with a purely repulsive core.

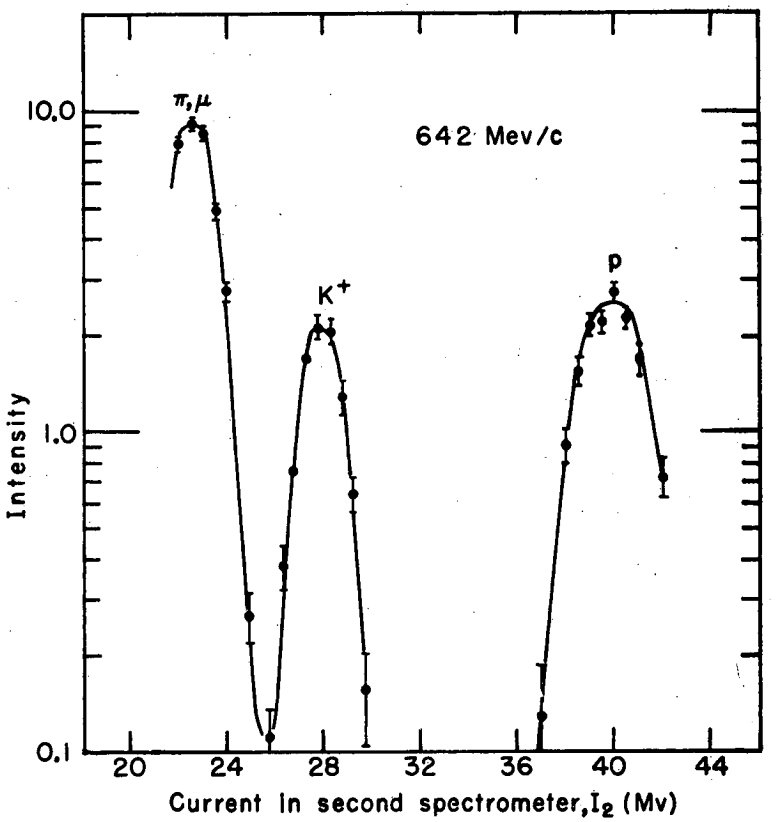
10.0
1.0
0.1
Intensity
π,μ
642 Mev/c
K+
p
20
24
28
32
36
40
44
Current in second spectrometer, I2 (Mv)
MU-21150

Fig. 1

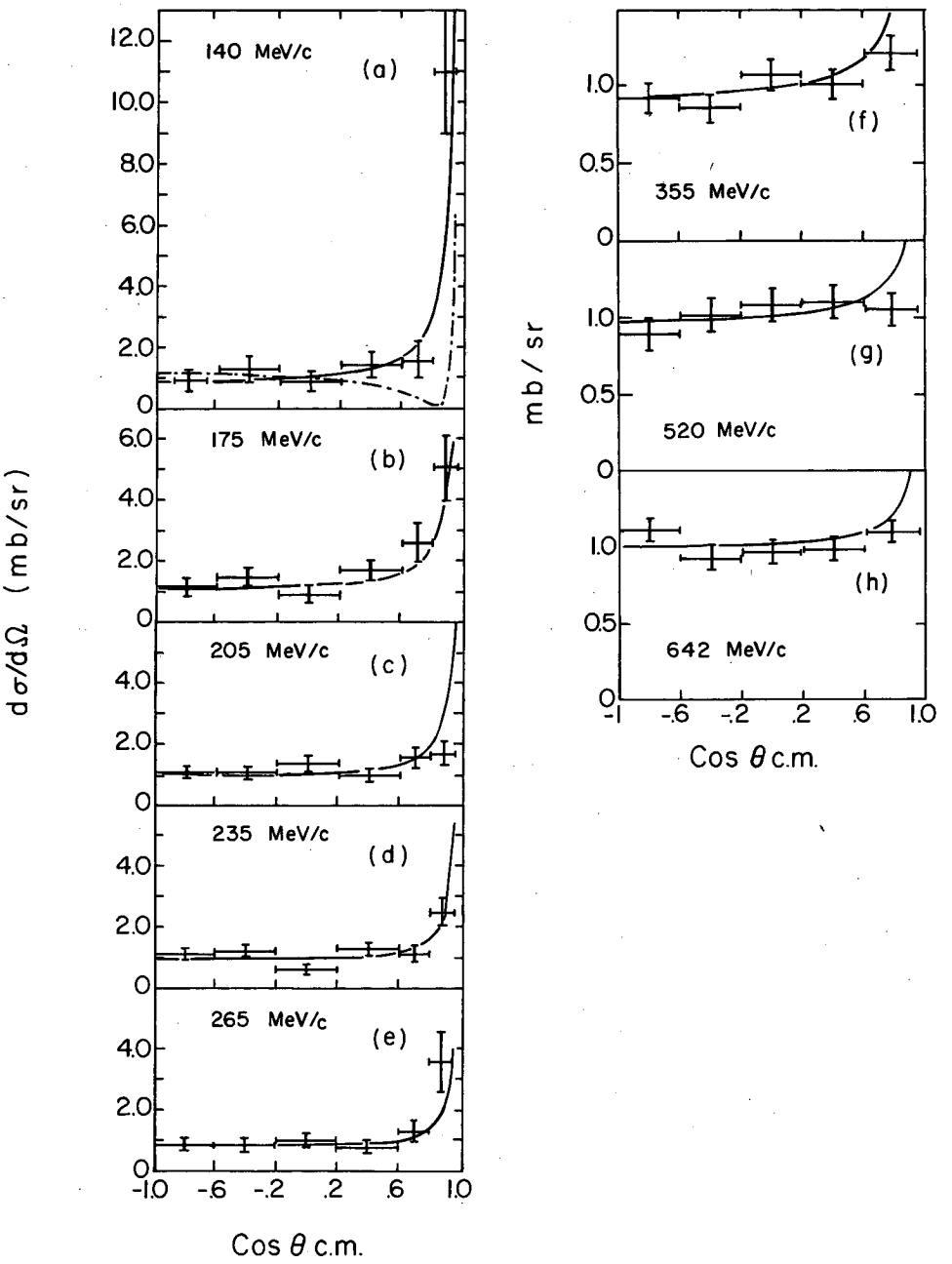
140 MeV/c
(a)
175 MeV/c
(b)
205 MeV/c
(c)
235 MeV/c
(d)
265 MeV/c
(e)
dσ/dΩ (mb/sr)
Cos θ c.m.
(f)
355 MeV/c
(g)
520 MeV/c
(h)
642 MeV/c
mb / sr
Cos θ c.m.
MUB-1156

Fig. 2

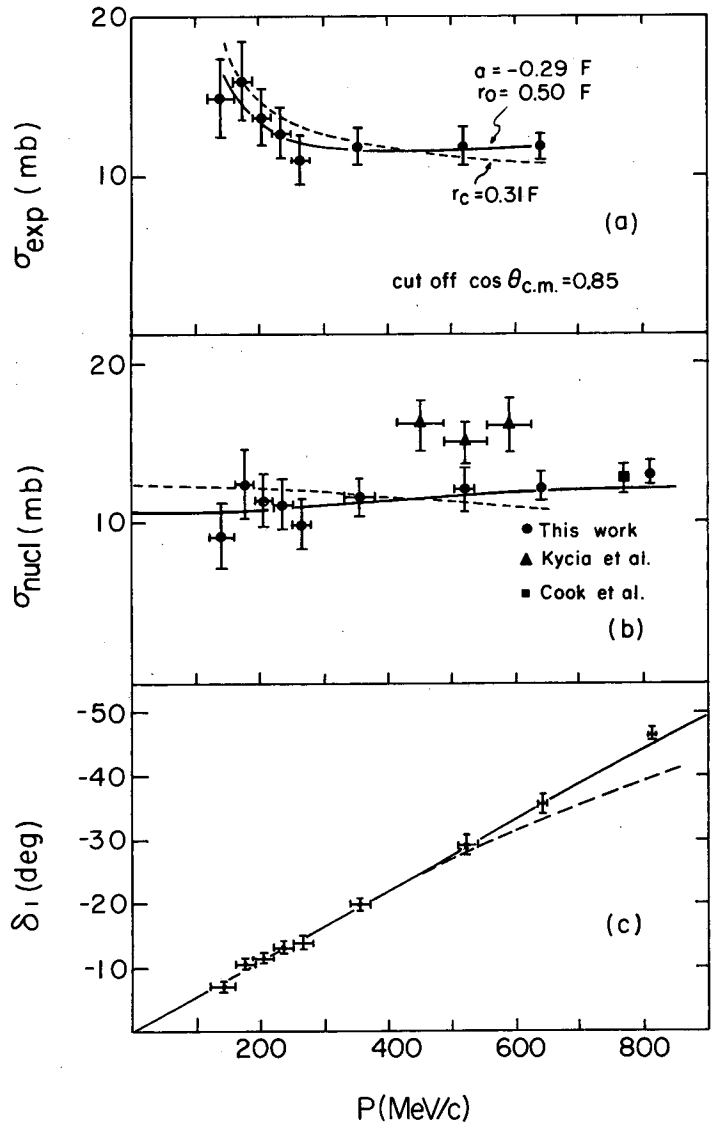

MU-27134

Fig. 3